第 48 卷 第 24 期/2021 年 12 月/中国激光 研究论文

中国激光

基于非绝热型微光纤的高灵敏度磁场传感器

齐晨英，徐常平，白扬博，李斌，苗银萍*

天津理工大学天津市薄膜电子与通信器件重点实验室，电气电子工程学院，天津 300384

摘要 利用熔接机电弧放电和氢气火焰加热相结合的方法，在光纤直径骤减的锥区中心位置制得非绝热型微光纤。该光纤结构具有较强的倏逝场，可以大幅增强光与物质的相互作用。将其与磁流体进行集成，基于磁流体的磁场可调谐折射率变化特性，能够实现对外界弱磁场的快速测量。研究结果表明，在 0～150 Oe 的磁场强度范围内，灵敏度可达 193.28 pm/Oe，探测极限约为 0.187 Oe，并且其灵敏度随着干涉峰波长的增大而增大。该传感器具有体积小、成本低、制作方法简单等优点，在电磁场检测领域具有良好的应用前景。

关键词 光纤传感器；磁场检测；磁流体；非绝热型；微光纤

中图分类号 O436 **文献标志码** A **doi**：10.3788/CJL202148.2406003

1 引 言

由于电磁场本身会对电子器件系统产生强烈的干扰和影响，对其在线检测一直是传感器与检测技术领域的难题。而且，一般需要进行电磁场测量的环境条件都比较恶劣，这无疑对传统的传感器与检测技术的有效检测增加了难度。光纤磁场传感器具有体积小、灵敏度高、环境适应能力强等优势，能够适应高温、核辐射、电磁干扰等高危环境，因此，在电磁场的在线检测领域具有很好的应用潜力。

光纤磁场传感器的主流方式是通过引入特殊介质使光和磁场发生法拉第(Faraday)旋光效应[1-2]，再将光纤与磁致伸缩材料[3-4]和磁流体(MF)[5-6]等磁场敏感材料结合。磁流体是一种新型的功能材料，具有折射率可调特性、双折射特性和透光率可调特性[5-9]。它既具有固体磁性材料特性，又具有液体的流动性，且易于与光纤集成。基于磁流体的光纤传感器能够避免传统采用块状磁光材料中的法拉第效应，改善集成光波导式磁场传感器中由于存在各种光路耦合、反射、对准而导致的制作工艺复杂及系统性能不稳定等技术缺陷。目前已报道的该类型传感器包括光栅型[10-12]、光子晶体光纤型[13-14]、干涉型光纤传感结构[Sagnac 型、迈克耳孙型、法布里-珀罗(F-P)型和马赫-曾德尔(M-Z)型[15-21]等]。其中，在线型 M-Z 光纤磁场传感器由于制作简单、结构紧凑、灵敏度高、成本低而备受关注。

2013 年，Wang 等[22]提出了一种灵敏度为 16.86 pm/Oe 的单模-多模-单模光纤结构，其中 1 Oe≙79.578 A/m。2015 年，Luo 等[23]提出了一种采用微光纤耦合器的磁场传感器，灵敏度为 191.8 pm/Oe，0.037 dB/Oe。2017 年，Pu 等[24]提出了基于 Sagnac 环和微光纤结谐振腔两种耦合结构的磁场传感器，灵敏度分别为 19.4 pm/Oe 和 171.8 pm/Oe。2018 年，Layeghi 等[25]提出基于锥形高双折射光纤的光纤环镜磁场传感器，灵敏度为 40.2 pm/Oe(402 pm/mT)。2018 年，Chen 等[26]提出了一种多模-单模-多模光纤结构，灵敏度为 −288.6 pm/Oe(−2.886 nm/mT)，−0.8 dB/Oe(−8.0 dB/mT)。2019 年，Zhang 等[27]提出了一种双锥串联 Bragg 光栅的磁场传感器，灵敏度为 40.782 pm/Oe(407.82 pm/mT)。2020 年，Wang 等[28]提出了一种光子晶体光纤与 Bragg 光栅串联的磁场传感器，灵敏度为 92.463 pm/Oe(924.63 pm/mT)。2020 年，Li 等[29]通过在单模光纤上先拉锥再刻蚀光栅，最后制成光纤磁场传感器，该传感器随磁场增

收稿日期：2021-02-03；**修回日期**：2021-04-24；**录用日期**：2021-06-02

基金项目：国家自然科学基金(11874281)、天津市自然科学基金重点项目(17JCZDJC31700，18JCTPJC49200)

通信作者：*kikosi@126.com

强和减弱时的灵敏度分别为 −0.1933 dB/Oe 和 −0.1533 dB/Oe。

这些研究表明，增强模式耦合或增加耦合区域长度，都可以提高微光纤传感器的灵敏度。对于非绝热型微光纤，当其直径急剧减小时，其在锥形区域会发生强耦合，部分纤芯基模会耦合到包层中以高阶均匀辐射模的形式进行传输。然而，直径的急剧变化导致耦合区域长度变短，限制了倏逝场；对于光纤直径缓慢减小的情况，光纤中各模式之间发生强耦合比较困难。

本文利用熔接机电弧放电拉锥和氢气火焰加热拉制相结合的方法，在光纤直径骤减的锥区中间制得一段细长且均匀的非绝热型微光纤。该光纤结构具有较强的倏逝场，可大幅增强光场与外场的相互作用[30]，因此，其对外界环境物理参量的变化更为敏感。将其与磁流体进行集成，基于磁流体磁场可调谐折射率变化的特性，实现了对外界弱磁场的高灵敏测量。该传感器具有体积小、成本低、制作方法简单等优点，在电力系统的磁场检测领域具有很大的应用潜力。

2　工作原理

2.1　基于光纤倏逝场的传感原理

光纤中的传输光在纤芯和包层表面发生全反射，产生倏逝波，其在包层介质中的有效透射深度 d_p 可表示为

$$d_p=\frac{\lambda_0}{2\pi}\frac{1}{\sqrt{n_1^2\sin^2\theta_i-n_2^2}},\tag{1}$$

式中 θ 为入射角，n_1 和 n_2 分别为纤芯和周围介质的折射率。通过(1)式可得，当固定入射角 θ 时，周围介质的折射率越小，能量的传输损耗越大。利用这一原理，将磁流体与微光纤进行集成，其包层环境即为磁流体。当磁流体的折射率改变时，倏逝波能量会随之发生一定的变化，通过分析传输信号光能量的改变可以实现磁场的测量。

2.2　磁流体的光学特性

磁流体的折射率可以通过调节外部施加的磁场强度来改变。这是由于磁流体在外部磁场作用下会出现固相与液相分离的状况，从而导致有效介电常数的改变，进而改变折射率的大小。根据 Langevin 理论，磁流体的折射率与所施加的磁场之间的关系为[31]

$$\varepsilon_{MF}=\frac{-\varepsilon_{col}(1-f)-\varepsilon_{hp}(f-1)+\sqrt{[\varepsilon_{col}(1-f)+\varepsilon_{hp}(f-1)]^2+4(1+f)^2\varepsilon_{col}\varepsilon_{hp}}}{2(1+f)},\tag{2}$$

式中 ε_{MF} 为磁流体有效介电常数，ε_{col} 与 ε_{hq} 为固相与液相的介电常数，f 为磁纳米颗粒分布系数。ε_{col} 为常数，ε_{hq} 随着外加磁场强度的变化而变化，满足

$$\varepsilon_{hq}\,|\,M_{s,eff}(H)=n_{MF}^2(M_s\,|\,H=0)=(0.1573M_s+1.3283)^2,\tag{3}$$

式中 $M_{s,eff}$ 为磁流体的有效浓度，M_s 为初始浓度。磁纳米颗粒分布系数 f 满足

$$f=(A_{col}/A)(1-A_{col}/A),\tag{4}$$

式中 A 和 A_{col} 分别为磁流体和磁链所占区域，两者均随外加磁场的变化而改变。已知磁流体的有效介电常数与折射率 n_{MF} 满足

$$n_{MF}=\sqrt{\varepsilon_{MF}}。\tag{5}$$

(5)式与(2)式和(4)式结合，可得到磁流体折射率随外加磁场变化的关系。

在微光纤结构的两个突变的锥区，一部分基模能量将耦合入包层模中，Lacroix 等[32]将突变型光纤锥看作模式干涉仪，即

$$I_m=I_1+I_2+2\sqrt{I_1I_2}\cos\varphi,\tag{6}$$

式中：$I_m(m=1,2)$ 是基模和包层模的光强；φ 是其相位之差，$\varphi=\Delta\beta L$，L 表示均匀锥区长度，传播常数差值 $\Delta\beta$ 的表达式为[33]

$$\Delta\beta=\frac{\lambda[(U_2^\infty)-(U_1^\infty)^2]}{4\pi n_1r^2}\exp\left(-\frac{2}{V}\right),\tag{7}$$

其中 $V=(2\pi r/\lambda)\sqrt{n_1^2-n_0^2}$ 表示归一化频率，n_1 表示光纤包层的折射率，n_0 表示外界环境的折射率，λ 代表真空中光的波长，r 表示均匀锥区的半径，U_1^∞ 和 U_2^∞ 表示两个干涉模式 U 值的极限值。

透射光谱中两个相邻干涉峰/谷之间的距离，即自由光谱范围(FSR，R_{FSR})，其与波长 λ 以及 n_0 之间的关系为

$$R_{FSR}(\lambda)=\frac{2\pi}{\partial\varphi/\partial\theta}=\frac{8\pi^2r^2n_1}{L[(U_2^\infty)^2-(U_1^\infty)^2]\left(1-\frac{2}{V}\right)\exp\left(-\frac{2}{V}\right)}。\tag{8}$$

结合(6)式和(7)式，可以求得外界折射率变化时干涉峰的波长变化灵敏度，即

$$\frac{d\lambda}{dn_0}=-\frac{\partial\varphi/\partial n_0}{\partial\varphi/\partial\lambda}=\frac{2\lambda n_0}{(V-2)(n_1^2-n_0^2)}。\tag{9}$$

根据（9）式，当 $n_0=1.4$，$n_1=1.4628$ 时，对于 $\lambda=1561$ nm 处的谐振峰，可得理论上的灵敏度约为 193.8 pm/Oe。

3　实验过程

3.1　非绝热型微光纤的制备

文中非绝热型微光纤的制备步骤包括：1）利用熔接机电弧放电，在单模光纤上制备两个级联的凹锥结构；2）将已制得的凹锥结构单模光纤固定在火焰拉锥机的马达上，继而手动调整，使氢气火焰对准凹锥结构后进行拉制，利用光谱仪实时观测微光纤制备过程中的光谱变化情况。所制备的微光纤结构光学显微照片如图 1（a）所示，图中 d_t 表示光纤锥区直径，d_w 表示光纤腰区直径。最后用玻璃毛细管对制备的微光纤结构进行磁流体封装，从而得到光纤磁场传感单元。图 1（b）为通过 Comsol 对光纤进行仿真计算得到的微纳光纤倏逝场能量占比情况，其倏逝场能量占比为 19.47%，这说明该光纤结构可以有效地与外界环境相互作用。在微纳光纤拉制中，随着锥区长度的增加，微纳光纤半径不断减小。改变微纳光纤半径，仿真计算可得，当半径从 2.68 μm 减小至 2.18 μm 时，倏逝场能量占比从 21.72%增至 34.34%。考虑到磁流体的虚部，锥区长度 L 越长，传感器损耗越大。

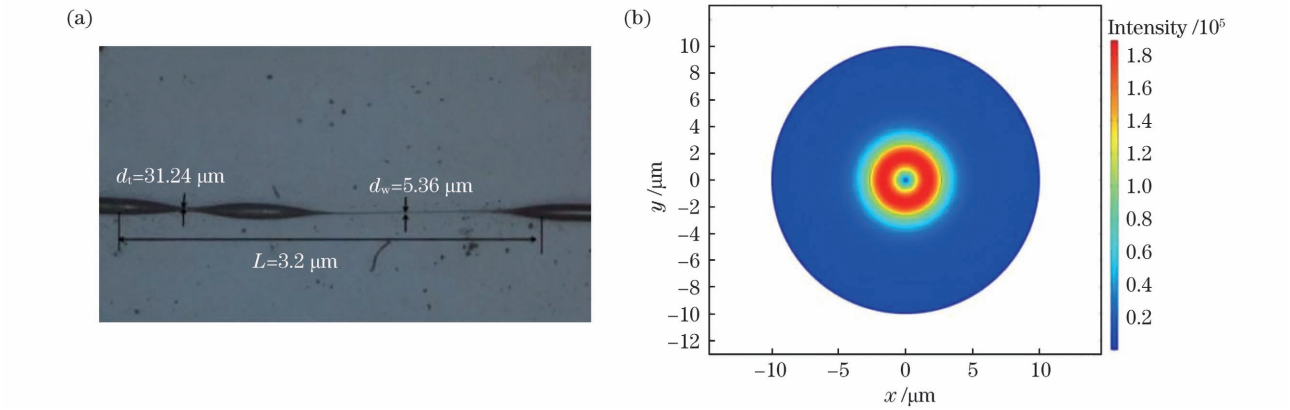

图 1　微光纤结构显微镜照片和 Comsol 仿真微光纤模场图。（a）微光纤结构显微镜照片；（b）Comsol 仿真微光纤模场图

Fig. 1　Microscopic photo of micro-fiber structure and Comsol simulated mode field of micro-fiber. (a) Microscopic photo of micro-fiber structure; (b) Comsol simulated mode field of micro-fiber

3.2　实验装置

实验装置示意图如图 2 所示。两个电磁铁产生均匀磁场，可调谐电压源（TVS）用来控制电磁铁的通电电流强度，超连续光源（SBS：光谱范围从 600 nm 至 1700 nm）用作光源，光谱分析仪（OSA：Yokogawa AQ6370C）用于检测输出光信号，其分辨率为 0.02 nm，高斯计用于探测磁场强度。其中磁流体（MF，EMG705：Ferrotec，Inc.）的饱和磁化强度约为 200 Oe、外部磁场强度为 0 时，该磁流体的初始折射率约为 1.40，MF 的密度为 1.18 g/cm^3，体积分数约为 3.9%。

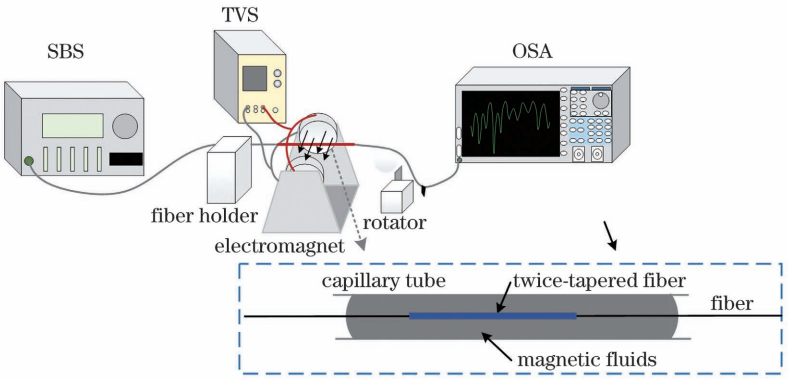

图 2　实验装置示意图

Fig. 2　Schematic diagram of experimental device

4 结果与分析

实验中磁场方向与光传输方向相互垂直。图 3 给出外部磁场强度为 0 时结构被磁流体封装前后的透射谱变化。从图中可以看出，当微光纤与磁流体集成之后，透射光谱相邻干涉峰之间的距离有所增大，这是由于传感结构的外部环境由空气变为磁流体后折射率增大所致。通过(8)式可以看出，FSR 将随外界折射率 n_0 与入射光波长 λ 的增大而展宽；并且对比封装前后的两个透射光谱发现，其所有相邻两个干涉峰之间的距离都是随着波长的增大而增加的，光谱的变化与理论分析相符合。

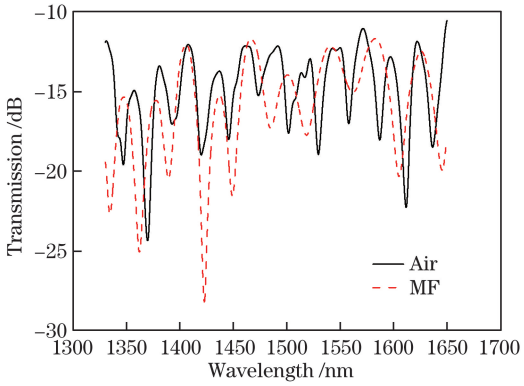

图 3 磁流体封装前后单模微光纤结构的透射光谱图

Fig. 3 Transmission spectrum of single-mode micro-fiber structure before and after magnetic fluid encapsulation

图 4 为外加磁场强度变化时的透射光谱，在磁场强度增大的过程中光谱整体向长波长处漂移，即发生了红移。当磁场强度在 0～30 Oe 区域变化时，透射光谱基本保持不变，原因是磁场强度小，导致对纳米颗粒的作用太弱而无法改变纳米颗粒的排列，进而使得磁流体折射率变化很小，波长漂移不明显。对透射光谱的 7 个干涉峰进行分析，所得干涉峰波长漂移与外界磁场对应关系如图 5 所示。当磁场强度在 0～150 Oe 区域变化时，7 个干涉峰分别在干涉波长位置 1362，1389，1422，1449，1484，1517，1561 nm 处获得为 65.65，75.07，85.03，100.35，135.7，166.06，193.28 pm/Oe 的磁场强度灵敏度。通过多次测量并对透射光谱进行分析，得到信号标准差为 12.06 pm，当灵敏度(S)为 193.28 pm/Oe 时，探测极限可达 0.187 Oe，品质因数 Q 为 8.77×10^{-3} Oe^{-1}。另外，可以通过提高磁流体材料的阈值来扩大对磁场强度的测量范围。由于磁流体的热光系数约为 -2.4×10^{-4} $℃^{-1}$，而磁流体折射率随外界磁场的变化系数约为 3×10^{-2} mT^{-1}，故温度的影响远小于磁场对其折射率的影响。即在温度变化较大时，温度引起的光谱变化远小于磁场改变时引起的光谱变化，因此，外界温度变化对传感器的影响不大。

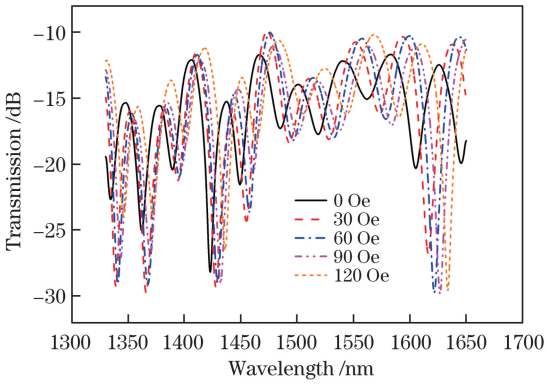

图 4 外加磁场强度变化时的透射光谱

Fig. 4 Transmission spectrum whit the applied magnetic field intensity changes

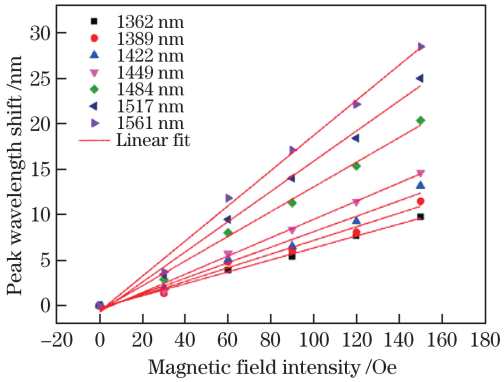

图 5 干涉峰波长位移与外界磁场的对应关系

Fig. 5 Relationship between interference peak wavelength shift and external magnetic field

由图 5 还可以看出，干涉峰的磁场强度灵敏度随着对应波长的增大而增大。图 6 是干涉峰的磁场强度灵敏度与其对应波长的关系，线性拟合得到的灵敏度是 0.67779 pm·Oe^{-1}·nm^{-1}，拟合系数 $R^2=0.9609$。可以看出，干涉峰的磁场强度灵敏度与其波长几乎呈线性关系。

由于本文中所设计的传感单元相当于一个多模式干涉仪，因此光纤参数 $V>2.405$，此时 $d\lambda/dn_0>0$。通过(9)式与归一化频率 V 的表达式可以看出，$d\lambda/dn_0$ 的值随波长 λ 与外界折射率 n_0 的增大而增大，或者随锥区半径 r 的减小而增大。图 6 所示的波长漂移量也从实验的角度验证了这一结论。通过上述理论分析与实验验证可得，若需要提高传感器件的灵敏度，可以通过使工作波长位于长波段，或者继续减小微光纤的直径来实现。

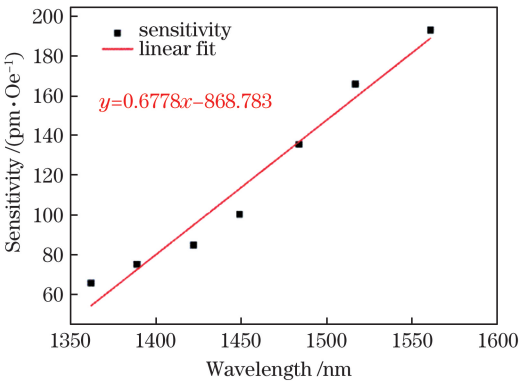

图 6 干涉峰的磁场强度灵敏度与其对应波长

Fig. 6 Magnetic field intensity sensitivity of interference peak versus its corresponding wavelength

5 结 论

提出一种基于微光纤与磁流体集成的高灵敏度磁场传感器。利用熔接机电弧放电和氢气火焰加热相结合的方法，在光纤直径骤减的锥区中心区域制得一段细长且均匀的非绝热型微光纤。该光纤结构具有较强的倏逝场，可以大幅加强光场与外场的相互作用，因此，对外界环境物理参量的变化较为敏感。通过将其与磁流体进行集成，基于磁流体的磁场可调谐折射率变化特性，实现了对外界弱磁场的测量。研究结果表明，在 0～150 Oe 的磁场强度变化范围内，灵敏度为 193.28 pm/Oe，探测极限约为 0.187 Oe。进一步研究表明，通过减小微光纤的直径以及增加其长度可大幅提升传感器的性能。该传感器具有体积小、成本低、制作方法简单等优点，在智能电网的电磁场在线监测、探矿工程、探测磁场源等领域具有强大的应用潜力。

参 考 文 献

[1] Bai Z Y, Zhang W G, Gao S C, et al. Compact long period fiber grating based on periodic micro-core-offset [J]. IEEE Photonics Technology Letters, 2013, 25(21): 2111-2114.

[2] Andre R M, Biazoli C R, Silva S O, et al. Strain-temperature discrimination using multimode interference in tapered fiber [J]. IEEE Photonics Technology Letters, 2013, 25(2): 155-158.

[3] Frazão O, Martynkien T, Baptista J M, et al. Optical refractometer based on a birefringent Bragg grating written in an H-shaped fiber [J]. Optics Letters, 2008, 34(1): 76-78.

[4] Ni X J, Huang M. Faraday effect optical current/magnetic field sensors based on cerium-substituted yttrium iron garnet single crystal [C]// 2010 Asia-Pacific Power and Energy Engineering Conference, March 28-31, 2010, Chengdu, China. New York: IEEE Press, 2010: 1-4.

[5] Cheng L H, Han J L, Guo Z Z, et al. A novel miniature magnetic field sensor based on Faraday effect using a heterodyning fiber grating laser [C]// 2012 Photonics Global Conference (PGC), December 13-16, 2012, Singapore. New York: IEEE Press, 2012: 1-4.

[6] Baudendistel T A, Turner M L. A novel inverse-magnetostrictive force sensor [J]. IEEE Sensors Journal, 2007, 7(2): 245-250.

[7] Chieh J J, Yang S Y, Chao Y H, et al. Dynamic response of optical-fiber modulator by using magnetic fluid as a cladding layer [J]. Journal of Applied Physics, 2005, 97(4): 043104.

[8] Deng H D, Liu J, Zhao W R, et al. Enhancement of switching speed by laser-induced clustering of nanoparticles in magnetic fluids [J]. Applied Physics Letters, 2008, 92(23): 233103.

[9] Liu T, Chen X, Di Z, et al. Tunable magneto-optical wavelength filter of long-period fiber grating with magnetic fluids [J]. Applied Physics Letters, 2007, 91(12): 121116.

[10] Miao Y P, Zhang H, Lin J C, et al. Simultaneous measurement of temperature and magnetic field based on a long period grating concatenated with multimode fiber [J]. Applied Physics Letters, 2015, 106(13): 132410.

[11] Zhang Z C, Guo T, Zhang X J, et al. Plasmonic fiber-optic vector magnetometer [J]. Applied Physics Letters, 2016, 108(10): 101105.

[12] Shi J M, Zheng D, Pan W, et al. Fiber grating ultrasonic sensor based on coupling cone structure and its application in nondestructive detection [J]. Acta Optica Sinica, 2019, 39(12): 1206004.
史镜名, 郑狄, 潘炜, 等. 基于耦合锥结构的光纤光栅超声波传感器及其无损检测研究 [J]. 光学学报, 2019, 39(12): 1206004.

[13] Gao R, Jiang Y, Abdelaziz S. All-fiber magnetic field sensors based on magnetic fluid-filled photonic crystal fibers [J]. Optics Letters, 2013, 38(9): 1539-1541.

[14] Wang C C, Fan R H, Wu G Z, et al. Characteristics of all-optical-fiber magnetic field sensor based on magnetic fluid coating and cooling tapering [J]. Laser & Optoelectronics Progress, 2020, 57(1): 010602.
汪成程, 范荣华, 吴根柱, 等. 基于磁流包覆冷却拉锥全光纤磁场传感器特性研究 [J]. 激光与光电子学进展, 2020, 57(1): 010602.

[15] Zhang N M Y, Dong X Y, Shum P P, et al. Magnetic field sensor based on magnetic-fluid-coated

long-period fiber grating [J]. Journal of Optics, 2015, 17(6): 065402.
[16] Chen Y F, Han Q, Liu T G, et al. Optical fiber magnetic field sensor based on single-mode-multimode-single-mode structure and magnetic fluid [J]. Optics Letters, 2013, 38(20): 3999-4001.
[17] Zhao Y, Wu D, Lv R Q, et al. Magnetic field measurement based on the Sagnac interferometer with a ferrofluid-filled high-birefringence photonic crystal fiber[J]. IEEE Transactions on Instrumentation and Measurement, 2016, 65(6): 1503-1507.
[18] Li X L, Ding H. All-fiber magnetic-field sensor based on microfiber knot resonator and magnetic fluid [J]. Optics Letters, 2012, 37(24): 5187-5189.
[19] El Amili A, Souza M C M M, Vallini F, et al. Magnetically controllable silicon microring with ferrofluid cladding [J]. Optics Letters, 2016, 41(23): 5576-5579.
[20] Chen Y F, Han Q, Yan W C, et al. Magnetic-fluid-coated photonic crystal fiber and FBG for magnetic field and temperature sensing [J]. IEEE Photonics Technology Letters, 2016, 28(23): 2665-2668.
[21] Miao Y P, Wu J X, Lin W, et al. Magnetic field tunability of optical microfiber taper integrated with ferrofluid[J]. Optics Express, 2013, 21(24): 29914-29920.
[22] Wang H T, Pu S L, Wang N, et al. Magnetic field sensing based on singlemode-multimode-singlemode fiber structures using magnetic fluids as cladding[J]. Optics Letters, 2013, 38(19): 3765-3768.
[23] Luo L F, Pu S L, Tang J L, et al. Highly sensitive magnetic field sensor based on microfiber coupler with magnetic fluid [J]. Applied Physics Letters, 2015, 106(19): 193507.
[24] Pu S L, Mao L M, Yao T J, et al. Microfiber coupling structures for magnetic field sensing with enhanced sensitivity [J]. IEEE Sensors Journal, 2017, 17(18): 5857-5861.
[25] Layeghi A, Latifi H. Tunable ferrofluid magnetic fiber sensor based on nonadibatic tapered hi-Bi fiber in fiber loop mirror [J]. Journal of Lightwave Technology, 2018, 36(4): 1097-1104.
[26] Chen H, Shao Z H, Zhang X, et al. Highly sensitive magnetic field sensor using tapered Mach-Zehnder interferometer[J]. Optics and Lasers in Engineering, 2018, 107: 78-82.
[27] Zhang R, Pu S L, Li Y Q, et al. Mach-Zehnder interferometer cascaded with FBG for simultaneous measurement of magnetic field and temperature[J]. IEEE Sensors Journal, 2019, 19(11): 4079-4083.
[28] Wang J, Pei L, Wang J S, et al. Magnetic field and temperature dual-parameter sensor based on magnetic fluid materials filled photonic crystal fiber[J]. Optics Express, 2020, 28(2): 1456-1471.
[29] Li P F, Yan H T, Xie Z W, et al. An intensity-modulated and large bandwidth magnetic field sensor based on a tapered fiber Bragg grating[J]. Optics & Laser Technology, 2020, 125: 105996.
[30] Wang L Z, Li L J, Tong L M. Optical microfibers and their applications in mode-locked fiber lasers[J]. Acta Optica Sinica, 2019, 39(1): 0126011.
王利镇, 李林军, 童利民. 微纳光纤及其锁模激光应用[J]. 光学学报, 2019, 39(1): 0126011.
[31] Hong C Y, Horng H E, Yang S Y. Tunable refractive index of magnetic fluids and its applications [J]. Physica Status Solidi (c), 2004, 1(7): 1604-1609.
[32] Lacroix S, Gonthier F, Black R J, et al. Tapered-fiber interferometric wavelength response: the achromatic fringe[J]. Optics Letters, 1988, 13(5): 395-397.
[33] Cassidy D T, Johnson D C, Hill K O. Wavelength-dependent transmission of monomode optical fiber tapers[J]. Applied Optics, 1985, 24(7): 945-950.

High-Sensitivity Magnetic Field Sensor Based on Non-Adiabatic Micro-Fiber

Qi Chenying, Xu Changping, Bai Yangbo, Li Bin, Miao Yinping*

Tianjin Key Laboratory of Film Electronic & Communicate Devices, School of Electrical and Electronic Engineering, Tianjin University of Technology, Tianjin 300384, China

Abstract

Objective Electromagnetic fields have the substantial interference and influence on electronic device systems, and their online detection has been a persistent problem in sensor and detection technologies. Furthermore, the

environmental conditions for electromagnetic field measurement are challenging, and traditional sensors are huge and have poor anti-interference ability. Optical-fiber magnetic field sensors are compact and have high sensitivity and strong environmental adaptability, which can withstand high temperature, nuclear radiation and electromagnetic interference. Therefore, it has good application potential in online electromagnetic field detection. Magnetic fluid is a new type of functional material with an adjustable refractive index, birefringence and light transmittance. It combines the characteristics of solid magnetic material with the fluidity of a liquid, making it easy to integrate with optical fiber. In this study, we propose a non-adiabatic optical-fiber magnetic field sensor, which is made by combining arc discharge with hydrogen flame heating. It can realize the rapid and accurate measurement of an external weak magnetic field. The basic strategy and research results will help in the development of a new optical-fiber magnetic field sensor.

Methods First, two cascaded concave cones were fabricated on a single-mode fiber using arc discharge. The single-mode fiber with a concave cone structure was then fixed on the flame taper machine's motor, and the hydrogen flame was manually adjusted to align with the concave cone structure for drawing. The spectrum changes during the preparation of micro-fiber were observed in real time using a spectrometer. Then, the supercontinuum source is used as the light source, and the cone is placed between the two coils. The electrified coil produces a uniform vertical magnetic field, and the voltage changes the magnetic field intensity. The effect of magnetic field intensity on the wavelength shift was investigated using a spectrometer to analyse the spectrum with the change of the magnetic field intensity.

Results and Discussions The optical-fiber magnetic field sensor has high magnetic field sensitivity, with a maximum sensitivity of 193.28 pm/Oe, a detection limit of 0.187 Oe and a quality factor of 8.77×10^{-3} Oe^{-1} (Fig. 5). When the magnetic field intensity is 0～30 Oe, the transmission spectrum remains unchanged. This is because the magnetic field intensity is small, which makes the effect on the nanoparticles too weak to change the arrangement of nanoparticles, causing the refractive index of the magnetic fluid to change slightly, and the wavelength shift to be incomprehensible. The magnetic field sensitivity of the interference peak increases with the wavelength (Fig. 6). The experimental results show that if the sensor's sensitivity is improved, the working wavelength can be located in the long wavelength band, or the micro-fiber's diameter can be reduced. Furthermore, the measurement range of the magnetic field intensity can be expanded by increasing the threshold value of magnetic fluid material. Because the thermal optical coefficient of the magnetic fluid is approximately -2.4×10^{-4} $℃^{-1}$ and the refractive index of the magnetic fluid changes with the external magnetic field is approximately 3×10^{-2} mT^{-1}, the influence of temperature is considerably less than that of the magnetic field. That is, when the temperature changes greatly, the spectral change caused by temperature is considerably less than that caused by magnetic field change. Thus, the influence of external temperature change on the sensor is small.

Conclusions A high-sensitivity magnetic field sensor based on the integration of micro-fiber and magnetic fluid is proposed. A thin and uniform non-adiabatic micro-optical fiber is fabricated in the central region of the tapered region where the diameter of the fiber decreases sharply by combining arc discharge with hydrogen flame heating. The fiber structure has a strong evanescent field, which considerably improves the interaction between the light field and the external field. Therefore, it is more sensitive to the changes in the physical parameters of the external environment. Through integrating it with magnetic fluid, the measurement of an external weak magnetic field is realized based on the tunable refractive index of magnetic fluid. The results show that the sensitivity is 193.28 pm/Oe and the detection limit is approximately 0.187 Oe in 0–150 Oe. Further research shows that the sensor's performance can be greatly improved by reducing the diameter of the micro-fiber and increasing its length. The sensor has the advantages of compact, low cost and simple manufacturing approach, which has potential application potential in the fields of online monitoring of the electromagnetic field in a smart grid, prospecting engineering and detection of magnetic field source.

Key words optical-fiber sensor; magnetic field detection; magnetic fluid; non-adiabatic; micro-fiber

OCIS codes 060.2370; 060.2430; 060.4005